J Appl Electrochem (2012) 42:325–332
DOI 10.1007/s10800-012-0399-z

ORIGINAL PAPER

High surface area $LaNiO_3$ electrodes for oxygen electrocatalysis in alkaline media

C. O. Soares · M. D. Carvalho · M. E. Melo Jorge · A. Gomes · R. A. Silva · C. M. Rangel · M. I. da Silva Pereira

Received: 24 November 2011 / Accepted: 6 March 2012 / Published online: 16 March 2012

Abstract $LaNiO_3$ coatings on nickel-foam supports were prepared by brush painting. The electrochemical properties were investigated by cyclic voltammetry (CV) and electrochemical impedance spectroscopy (EIS). Comparative studies were performed with $LaNiO_3$-pelleted electrodes. The roughness factors were determined by CV and found to be 5,208 ± 350 and 4,037 ± 250 for the pelleted and coated electrodes, respectively. EIS measurements confirm the results obtained by CV. Values lower than 0.3 were calculated for the morphology factors for both electrodes, indicating low electrochemical porosity. The experimental method used in this work to synthesise the oxide coupled with the use of Ni foam as support has proved to be very effective in producing oxide electrodes with surface areas higher than those referred to in relevant literature.

Keywords $LaNiO_3$ films · Foam nickel support · Surface area · Cyclic voltammetry · Electrochemical impedance spectroscopy

1 Introduction

Perovskite-type oxides, with the general formula ABO_3, are catalysts of great diversity because of the wide range of ions and valences that the structure can accommodate. The bifunctional character of these materials is the subject of research in view of the need for alternatives to noble materials and of the paramount importance of electrode development for next generation of regenerative fuel cells.

For the design of practical electrocatalyst electrodes, reasonable electrical conductivity, durability, catalytic activity, selectivity and surface area are important factors. Large surface areas are usually associated with high catalytic activities, and strong dependence on the oxide and electrode preparation methods. In the case of oxide coatings, the support material is a key parameter. Several materials are widely used as supports, namely titanium, steel and nickel. With the aim of increasing the surface area, foam nickel substrates have been used with success for the electrodeposition of NiO films for lithium-ion batteries [1].

Nickel containing perovskite-type oxides have been reported among the most active materials for oxygen evolution reaction (OER) in alkaline media as well as demonstrating good electrocatalyst properties for oxygen reduction reaction (ORR) [2]. In particular, $LaNiO_3$ has been recognised as one of the most promising electrodes for oxygen evolution and reduction [3–12], and its potential use as bifunctional oxygen electrode [10, 13].

It is well known that the electrocatalytic activity depends on the oxide preparation method, namely, on the precursors, pH and synthesis temperature as well as on the electrode fabrication. Based on our experience in developing oxide electrocatalysts [14–20], the present study represents our continuing effort in search of more active bifunctional electrode materials. Previous studies on the catalytic activity towards the OER in alkaline medium showed that an increase on the electrode activity, when compared with relevant published data, is mostly related to

C. O. Soares · M. D. Carvalho · M. E. Melo Jorge · A. Gomes · M. I. da Silva Pereira (✉)
Departamento de Química e Bioquímica, C.C.M.M., Faculdade de Ciências, Universidade de Lisboa, Campo Grande 1749-016, Lisboa, Portugal
e-mail: mipereira@fc.ul.pt

R. A. Silva · C. M. Rangel
Fuel Cells and Hydrogen Unit, Laboratório Nacional de Energia e Geologia, Paço do Lumiar 22, 1649-038 Lisbon, Portugal

geometric factors [20]. This report covers a study on the electrochemical properties of $LaNiO_3$ electrodes in the form of coating on nickel-foam supports. It is expected that the nickel-foam can give dimensional stability to the electrode material, low contact resistance between the oxide and support and possibility of high loading of metal oxide. Consequently, it may play a favourable role in improving higher catalytic activity of the oxide electrode.

A similar study was performed on $LaNiO_3$-pelleted electrodes for comparison purposes.

2 Experimental

The perovskite-type oxide $LaNiO_3$ was prepared by a self-combustion method using citric acid, as previously reported [20]. Stoichiometric amounts of La_2O_3 (99.95 %, Sigma Aldrich), previously heated at 1,173 K and Ni (99.99 %, Sigma Aldrich) were separately dissolved in HNO_3 (69 %, Sigma Aldrich). Citric acid (99 %, Sigma Aldrich) was added in equal amount to the total metal ions. The solution was heated up on a sand bath with consequent degradation and combustion of the resulting gel. The dry product obtained was heated at 873 K for 6 h to remove the residual organic matter, and the resulting powder was finally heated at 1,173 K in air for 12 h.

Structural characterisation was performed by X-ray diffraction (XRD) using a Philips PW 1730 diffractometer, operating with Cu Kα radiation. The cell parameters were calculated by the Unit cell program [21].

The films were prepared by coating (brush painting) a nickel-foam support (Goodfellows, 1.6-mm thickness, 95 % porosity and 20 pores cm^{-1}), typically 0.5×0.5 cm^2, with a suspension of the oxide in TritonX-100 Fluke Chemie AG. After each application, the solvent was evaporated and the dried layer fired, in an oven, until temperature reached 673 K followed by 3 h at 673 K. The oxide loading was controlled to be around 89 ± 5 mg cm^{-2}. With regard to the pelleted electrodes, the oxide powder (around 140 ± 8 mg) was uniformly distributed onto an inserted Pt mesh and pressed into 1 mm thick, 1 cm^2 platelet pellets under 40 bar pressure and sintered at 1,173 K in air for 6 h. The electrical contact was made by welding the Pt mesh to a silver wire. The samples were then mounted in a glass tube with araldite epoxy resin, so that the electrolyte could only make contact with the oxide. Three specimens were prepared for each type of electrodes, two for the electrochemical experiments and one for morphological characterisation.

The global aspect of the electrodes was observed by optical microscopy (Nikon SMZ 1500) and the morphology was observed using a Phillips scanning electron microscope, Model XL 30 FEG, coupled to an energy dispersive spectrometer, EDS. AFM-images were recorded in tapping mode in a nanoscope IIIa multimode microscope (Digital Instruments, Veeco). Measurements were performed in air using etched silicon cantilevers (RTESP, Veeco) with a resonance frequency of ca. 300 kHz.

On the electrochemical studies a conventional three-electrode glass cell was used. The measurements were carried out at room temperature, using Hg/HgO (+0.098 V vs. SHE) as the reference electrode and Ni foam as counter electrode. A potassium hydroxide 1 M solution (>90 %, Sigma Aldrich) was prepared using Millipore Milli-Q ultrapure water (18 M Ω cm). Before each electrochemical measurement, the KOH 1 M solution was purged with high-purity N_2.

A Voltalab 32 radiometer apparatus associated to an IMT 102 interface controlled by a personal computer through the VoltaMaster 2 software was used for the cyclic voltammetric studies.

The electrochemical impedance measurements were performed using a frequency response analyser (model 1250, Solartron) connected to an electrochemical interface (model 1286, Solartron).

Spectra were obtained at several points along the polarisation curve, in the potentiostatic mode. Impedance spectra were recorded at ten points per decade by superimposing a 10 mV ac signal typically over the frequency range from 25,000 to 0.001 Hz.

3 Results and discussion

3.1 Material characterization

The XRD pattern of the obtained product, presented in Fig. 1, allows for the identification of the perovskite-type

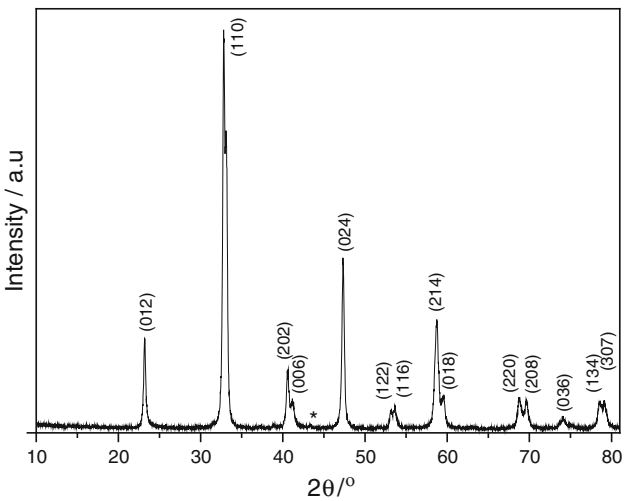

Fig. 1 X-ray diffraction pattern of the $LaNiO_3$ powder (*NiO traces)

phase, characteristic of the $LaNiO_3$ rhombohedral structure, although traces of NiO were also observed. The calculated cell parameter values ($a = 5.457$ Å and $c = 13.134$ Å) are in accordance with other published work [22].

Surface images of the nickel-foam support (a), oxide coating (b) and pellet (c), obtained by optical microscopy, are shown in Fig. 2. It is clear from these images that the surface and pore of the Ni foam support are covered and filled with the oxide presenting a few uncovered Ni points and an irregular surface. Conversely, the pellet exhibits a smooth surface, and almost no pores are detected. The observation with a scanning electron microscope (SEM) reveals the open porous morphology of the Ni foam (d) and a granular morphology for the coating (e) and pellet (f). Individual particles were not discernible, and the aggregates had irregular shapes. From these results it is reasonable to assume that both coating and pellet electrodes have very high electrode/electrolyte contact area which is beneficial for oxygen evolution anodes.

Figure 3 displays the 2D and 3D AFM-images of the surface of the $LaNiO_3$/Ni (a) and pelleted (b) electrodes. As can be seen, the perovskite films present globular-shaped grains, densely packed and well distributed on the Ni foam substrate, while the pellets show a more even surface. The electrodes'root-mean-square roughness (Rq) was determined in an area of 3.5×3.5 μm^2. The coating exhibits an Rq value of 336 higher than 233 nm found for the pellet. These values indicate that the pellet is slightly smoother than the coating in accordance with the recorded images.

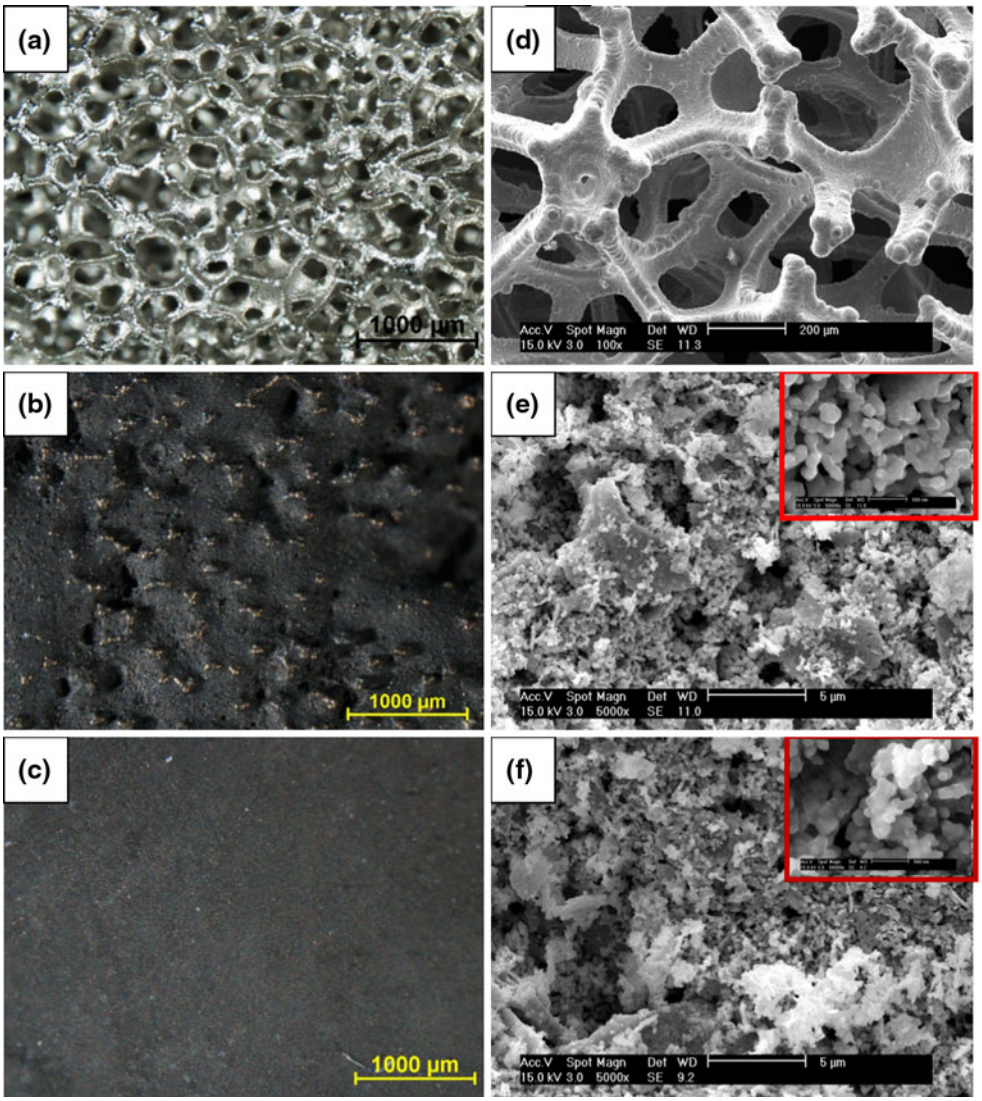

Fig. 2 Optical (×30) and SEM microscope images for Ni foam (**a**, **d**), $LaNiO_3$/Ni (**b**, **e**) and $LaNiO_3$ pelleted electrodes (**c**, **f**)

3.2 Open-circuit potential measurements

The open-circuit potential (E_{oc}) in 1 M KOH was recorded for pelleted and oxide-coated electrodes as well as for the Ni foam support and the values, after 24 h of immersion were 0.206, −0.112 and −0.152 V vs. Hg/HgO, respectively.

The E_{oc} of the pelleted electrode lies between the calculated thermodynamic potential for the redox couples Ni^{3+}/Ni^{2+} and $Ni^{3+}/Ni^{2.67+}$, 0.107 and 0.380 V vs. Hg/HgO, respectively [23]. This value can be understood in terms of the surface equilibrium of the redox couple Ni^{3+}/Ni^{2+}, depending on the ratio of the two species at the oxide surface. On the other hand, the E_{oc} for the coating is lower than the one for the pelleted electrode, approaching the value obtained for the Ni foam support. This result indicates a possible contact between the electrolyte and the Ni foam through the oxide pores.

3.3 Cyclic voltammetry

Electrochemical characteristics of the two kinds of electrodes were investigated by cyclic voltammetry (CV). Figure 4 presents typical stabilised cyclic voltammograms recorded for $LaNiO_3$-pelleted and coated electrodes in KOH 1 M at a sweep rate of 10 mV s^{-1}. A voltammogram for the Ni foam support is also presented. For all the electrodes, an anodic and the corresponding cathodic peak are observed, prior oxygen evolution, usually assigned to the redox pair Ni^{3+}/Ni^{2+} [6–9, 24]. For the oxide electrodes, another cathodic peak was observed, in the negative potential range around −0.025 V vs. Hg/HgO attributed to the oxygen reduction [10], which is more evident for the pelleted electrodes.

The average values of the peak potential, peak separation and estimated formal redox potential associated with

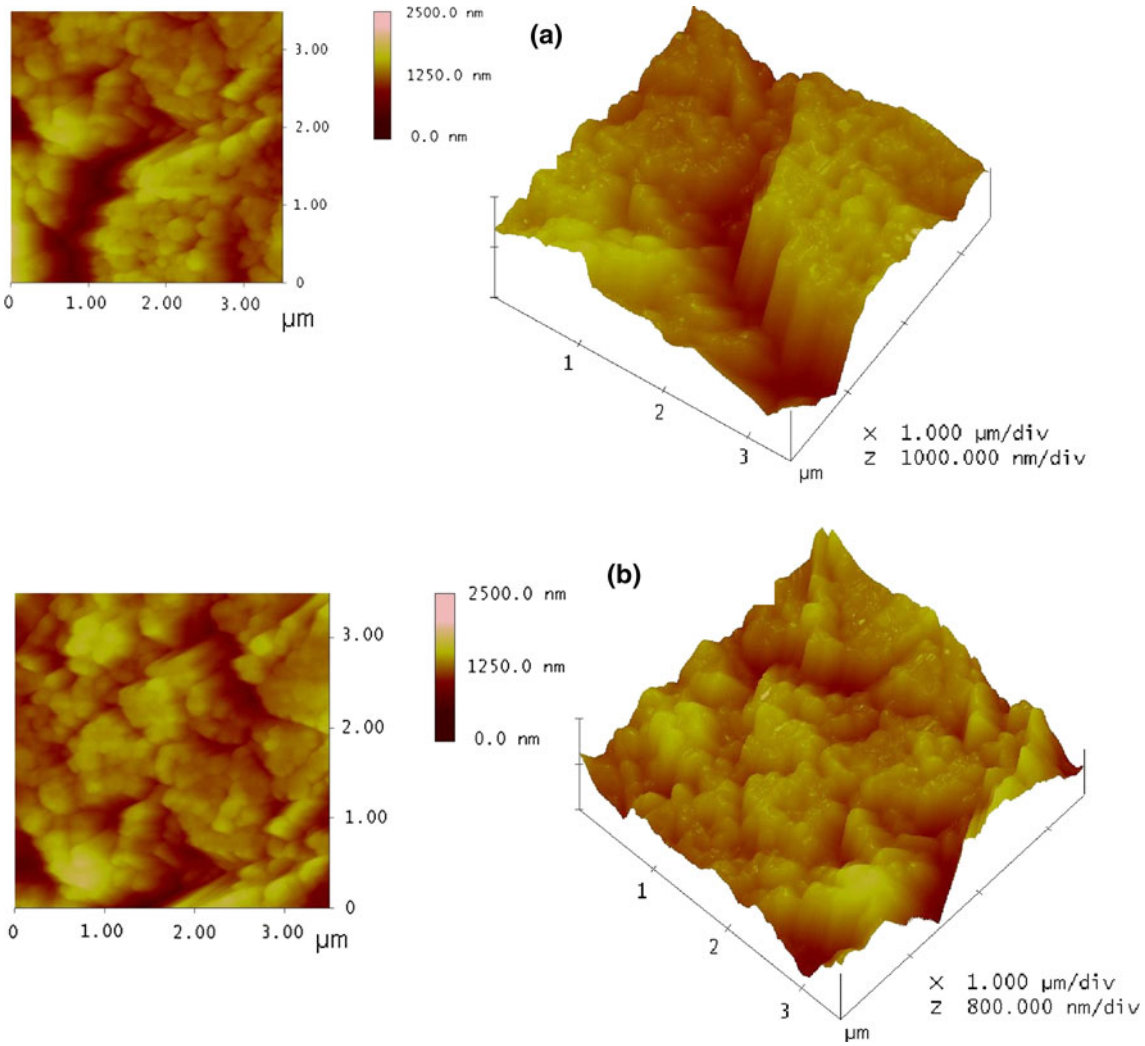

Fig. 3 AFM images of $LaNiO_3$/Ni (**a**) and $LaNiO_3$ pelleted electrodes (**b**)

this pair of peaks, for all the studied electrodes, are given in Table 1, where values from relevant literature were also included. The values for pelleted and coated $LaNiO_3$ electrodes are very similar, and consistent with the published ones, for the same oxide electrode [6, 7, 9]. The peak separation is analogous for the two kinds of electrodes suggesting comparable electrochemical reversibility. It can be noted, from the figure, that the current densities for the coating are much higher than those of the pelleted electrode, indicating a contribution from the Ni foam support, as a result of electrolyte contact with the substrate, through the pores, in accordance with the observed during open-circuit potential measurements.

3.4 Roughness and morphology factors

The electrode's capacitance has been estimated from the charging currents (i_{dl}) recorded between −0.050 and +0.050 V vs. Hg/HgO, where no faradaic currents were observed (Fig. 5a, b), at sweep rates (v) varying from 4×10^{-3} to 80×10^{-3} V s^{-1}. The voltammetric profiles show the typical capacitor-like characteristics in the form of almost rectangular cyclic behaviour (Fig. 5b). However, with the increase of sweep rate, the curves show a clear distortion at the switching potential due to solution and electrode resistance. The charging currents were measured for each sweep rate, at a potential located within the last 20 % of the potential interval covered, in accordance with the procedure proposed by da Silva et al. [25]. The plots

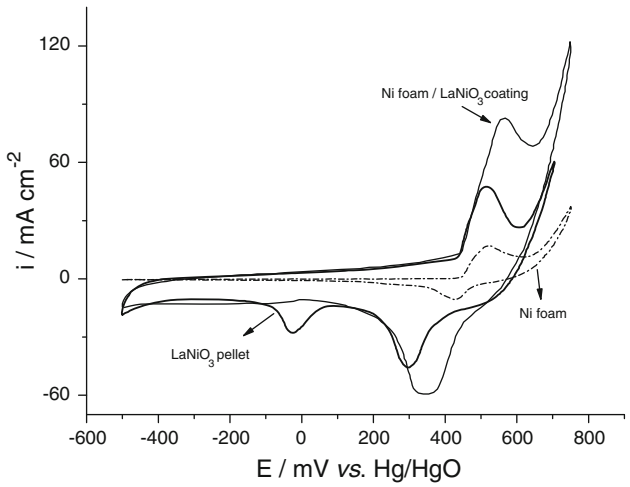

Fig. 4 Typical cyclic voltammograms recorded for Ni foam, $LaNiO_3$/Ni and $LaNiO_3$ pelleted electrodes in KOH 1 M at a sweep rate of 10 mV s^{-1}

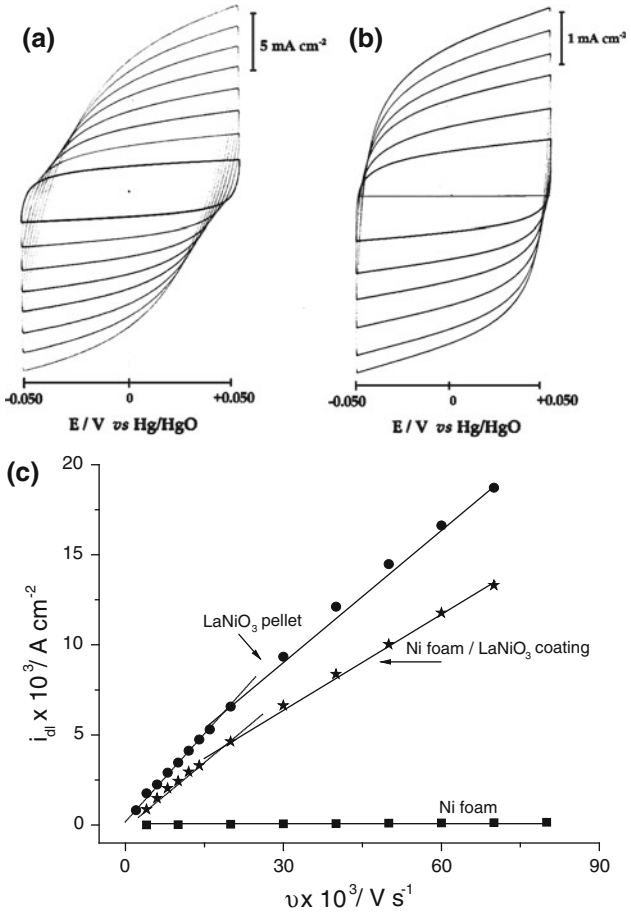

Fig. 5 Cyclic voltammograms in the double layer region (**a**, **b**) and charging current densities as a function of sweep rate (**c**) for a $LaNiO_3$ coated electrode in KOH 1 M. Sweep rates of 10, 20, 30, 40, 50, 60, 70, and 80 mV s^{-1}(**a**) and 4, 6, 8, 10, 12, and 14 mV s^{-1}(**b**)

Table 1 Averaged voltammetric parameters and roughness factors for $LaNiO_3$ electrodes, prepared by different methods, in alkaline solutions

Electrode	Preparation method	E_{pa}/V	E_{pc}/V	ΔE_p/V	$E^0 = (E_{pa} + E_{pc})/2$/V	R_f	References
Ni foam		0.522	0.423	0.099	0.472	90 ± 9	This work
$LaNiO_3$ pellet	Self-combustion	0.519	0.298	0.221	0.408	5,208 ± 350	This work
$LaNiO_3$/Ni	Self-combustion	0.568	0.354	0.214	0.461	4,037 ± 250	This work
$LaNiO_3$/Pt	Spray pyrolysis	0.505	0.410	0.095	0.457	170	[6]
$LaNiO_3$/Pt	Thermal decomposition	0.510	0.445	0.075	0.472	470	[6]
$LaNiO_3$/Ni	Thermal decomposition	0.530	0.380	0.150	0.455	666	[7]
$LaNiO_3$/Ni	Sol–gel	0.546	0.334	0.212	0.440	1,025	[9]

i_{dl} vs. v are presented in Fig. 5c, for the Ni foam, pelleted and coated electrodes. For the oxide electrodes two linear regions were observed for $v \leq 14 \times 10^{-3}$ V s^{-1} [$R^2 = 0.9936$ (coating) and $R^2 = 0.9968$ (pellet)] and $v > 20 \times 10^{-3}$ V s^{-1} [$R^2 = 0.9986$ (coating) and $R^2 = 0.9959$ (pellet)], respectively. On the other hand, for the Ni foam support, a linear variation was observed for the whole sweep rate range. According to da Silva et al. [25], the two linear regions can be correlated with the morphology of highly porous/rugged films and the change on the slope, for high sweep rates, to the exclusion of surface areas of more difficult access.

The double layer capacitance (C_{dl}) of the Ni foam support and $LaNiO_3$/1 M KOH interfaces was calculated from the slope of the linear regions for $v \leq 14 \times 10^{-3}$ V s^{-1}. The electrodes' roughness factor (R_f) was determined, using 60 and 20 μF cm^{-2} as the C_{dl} values for oxide [26] and metallic [27] smooth surfaces, respectively, and the values are displayed in Table 1. The coatings' roughness factor is much higher than those reported in relevant literature, for the same oxide (see Table 1). In fact, a large interval of R_f values are found in relevant literature, which is closely related with the oxide/electrode preparation conditions, being one of the most important factors controlling the overall behaviour of oxide electrodes [2, 28]. The clear enhancement of roughness for the coated electrodes, prepared in this work, can be associated with the electrode preparation method

Table 2 $LaNiO_3$/1 M KOH interface parameters

Electrode	Cyclic voltammetry				EIS	
	C_{dl}/F cm^{-2}	C_e/F cm^{-2}	C_i/F cm^{-2}	φ	C_{dl}/F cm^{-2}	R_f
$LaNiO_3$ pellet	0.312 ± 0.021	0.243 ± 0.016	0.070 ± 0.005	0.22	0.275 ± 0.015	4,583 ± 250
$LaNiO_3$/Ni	0.242 ± 0.015	0.173 ± 0.011	0.070 ± 0.004	0.29	0.185 ± 0.005	3,083 ± 83

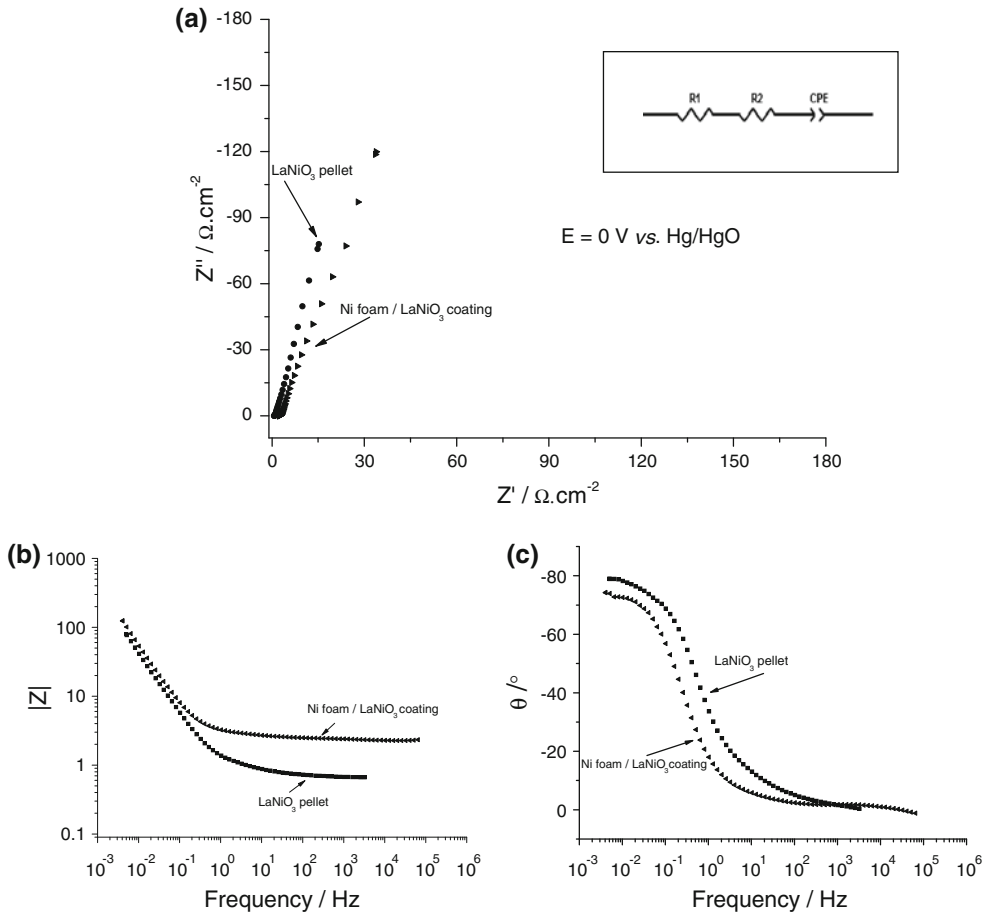

Fig. 6 Impedance data represented as Nyquist (**a**) and Bode plots (**b**, **c**) for $LaNiO_3$/Ni and $LaNiO_3$ pelleted electrodes in 1 M KOH at potentials of 0.0 V. *Inset*: Equivalent circuit used to model the data at low frequencies

coupled to the use of high oxide loadings and Ni foam as the oxide support.

The pellets are ≈29 % rougher than the coated electrodes, and the R_f compares well with the literature values ranging from 5,600 to 1,500 for the same type of electrodes [3, 29].

To evaluate the electrochemical porosity of the oxide surfaces the morphology factor, φ, defined as the ratio of the differential capacity of the internal region of the film (C_i) and the total differential capacity C_i/C_{dl}, has been determined [25]. The C_i values were obtained by subtracting the slopes of the linear segments of the i_{dl} vs. v plots for the low and high sweep rate regions (see Table 2). The calculated morphology factors for the coated and pelleted electrodes are 0.29 and 0.22, respectively. These low φ values (<0.3) indicate that the electrodes have a low electrochemical porosity. The enhanced roughness and low electrochemical porosity of the oxide electrodes can be explained by the major role played by the oxide/solution macroboundary (outer surface), with a small contribution of the oxide/solution microboundaries, due to the penetration of the solution into pores and intergrain regions (inner surface) [30]. Values varying from 0.41 to 0.82 are referred to in relevant literature for $LaNiO_3$/Ni-PVC electrodes in 1 M KOH depending on the conditions and time of cycling [11].

3.5 Impedance measurements

The double layer capacitance was also estimated for the two kinds of $LaNiO_3$ electrodes by electrochemical impedance spectroscopy (EIS) in the range of potentials from −0.050 to +0.050 V vs. Hg/HgO. Typical results are presented in Fig. 6. The response of the system was fitted so that deconvolution of the contributions from the capacitive and resistive components is made possible. To simulate the double layer of the electrode/electrolyte interface, the use of a simple capacitor is only acceptable in situations where the electrolyte is concentrated and the electrode can be considered smooth. In this case, results were modelled with an equivalent circuit in which the capacitance was replaced with a constant phase element (CPE) to reflect the geometrical effect. The impedance of the CPE is defined according to Eq. (1)

$$Z_{CPE} = \frac{1}{Y_0(jw)^n} \quad (1)$$

where Y_0 is the capacitance, j is the square root of −1, w is the frequency and n is the CPE ideality factor associated to the distortion of the capacitance due to electrode surface roughness. In order to compare the double layer values obtained by EIS with those obtained by CV, low frequency impedance data were selected to be modelled using an equivalent circuit which includes the pore impedance constituted by the pore resistance (R_2) and a constant phase element (CPE1) connected in series [31]. Data plotted in the complex plane (Fig. 6a), are characterised by a vertical line at low frequencies with a deviation from the ideal capacitive behaviour being less for the pellet electrode. Figure 6b, c show the Bode plots with phase angles between 75° and 80°. In the |Z| vs. frequency plot, the more resistive character of the Ni foam/$LaNiO_3$ coating is evident.

Table 3 Ratio between different morphologic parameters, obtained for the $LaNiO_3$ pelleted and coated electrodes

Method	R_f(pellet)/ R_f(coating)	φ(pellet)/ φ(coating)	Rq(pellet)/ Rq(coating)
Cyclic voltammetry	1.3	0.76	×
EIS	1.5	×	×
AFM	×	×	0.69

Table 2 shows estimated values of C_{dl} parameters found by EIS data for the coating and pellet $LaNiO_3$ electrodes using the equivalent circuit at low frequencies presented on the inset of Fig. 6a. The average double layer capacitances are in absolute value lower than those obtained by CV, but their ratio is the same, as Table 3 shows, yielding R_f values of the same order of magnitude. The pore resistance was also estimated with values of 0.169 ± 0.038 and $0.045 \pm 0.009\ \Omega\ cm^2$ obtained for the coating and pelleted electrodes, respectively.

On the other hand, the ratio between the morphology factors for the pelleted and coated electrodes is comparable to the ratio of the root-mean-square roughness estimated by AFM. This is a very interesting result that suggests that both techniques give similar information concerning the porous nature of the oxide electrode.

Comparing the roughness and morphology factors, for both electrodes, it can be concluded that the processes involved are mainly due to the reaction of OH^- ions at the oxide electrode surface:

$$LaNiO_{3-\partial}(OH)_{y+\partial} + \partial OH^- \leftrightarrow LaNiO_3(OH)_y + \partial H_2O + \partial e^- \quad (2)$$

Considering the size of the OH^- ion, it is not surprising that there is little bulk interaction due to the diffusion of OH^- ions into the oxide pores.

4 Conclusions

As a result of this work it can be concluded that Ni foam is suitable to use as support for oxide electrodes.

The experimental method used in this work to synthesise the oxide coupled with the use of Ni foam as support has proved to be very effective in producing oxide electrodes with surface area higher than those referred to in relevant literature.

This work also shows that CV is a convenient method for the assessment of porous oxide electrodes. The coupling of CV and AFM provides a suitable way of obtaining a more complete understanding of the oxide electrodes. EIS measurements confirm the results obtained by CV and they also give additional information about the porosity of the electrodes.

Overall, it can be said that this study has provided valuable insights into the methodology to prepare oxide electrodes with high surface area.

Acknowledgments This work was partially financed by Fundação para a Ciência e Tecnologia (FCT), under contract no. PTDC/CTM/102545/2008. C.O. Soares acknowledged a grant from FCT under the same contract.

References

1. Wang H, Pan Q, Wang X, Yin G, Zhao J (2009) J Appl Electrochem 39:1597
2. Kinoshita K (1992) Electrochemical oxygen technology, the electrochemical society series, 1st edn. Wiley, New York, pp 293–295
3. Otagawa T, Bockris JO'M (1984) J Electrochem Soc 131:290
4. Bockris JO'M, Otagawa T, Young V (1983) J Electroanal Chem 150:633
5. Bockris JO'M, Otagawa T (1982) J Electrochem Soc 129:2391
6. Singh RN, Bahadur L, Pandey JP, Singh SP, Chartier P, Poillerat G (1994) J Appl Electrochem 24:149
7. Singh SP, Singh RN, Poillerat G, Chartier P (1995) Int J Hydrog Energy 20:203
8. Singh RN, Jain AN, Tiwari SK, Poillerat G, Chartier P (1995) J Appl Electrochem 25:1133
9. Singh RN, Tiwari SK, Singh SP, Jain AN, Singh NK (1997) Int J Hydrog Energy 22:557
10. Tiwari SK, Koenig JF, Poillerat G, Chartier P, Singh RN (1998) J Appl Electrochem 28:114
11. González M, Elizalde MP, Baños L, Poillerat G, Dávila MM (1999) Electrochim Acta 45:741
12. Singh RN, Tiwari SK, Sharma T, Chartier P, Koenig JF (1999) J New Mater Electrochem Syst 2:65
13. Bursell M, Pirjamali M, Kiros Y (2002) Electrochim Acta 47:1651
14. Godinho MI, Catarino MA, da Silva Pereira MI, Mendonça MH, Costa FM (2002) Electrochim Acta 47:4307
15. Mendonça MH, Godinho MI, Catarino MA, da Silva Pereira MI, Costa FM (2002) Solid State Sci 4:175
16. Carvalho MD, Wattiaux A, Bassat JM, Grenier JC, Pouchard M, da Silva Pereira MI, Costa FMA (2003) J Solid State Electrochem 7:700
17. Ciríaco MLF, Silva Pereira MI, Nunes MR, Mendonça MH, Costa FM (2006) Mater Chem Phys 96:211
18. Lucas C, Eiroa I, Nunes MR, Russo PA, Ribeiro Carrot MML, da Silva Pereira MI, Melo Jorge ME (2009) J Solid State Electrochem 13:943
19. Pereira MIS, Melo MJBV, Costa FMA, Nunes MR, Peter LM (1989) J Chem Soc Faraday Trans 1(85):2473
20. Soares CO, Carvalho MD, Jorge MEM, Gomes A, Silva RA, Rangel CM, da Silva Pereira MI (2011) Port Electrochim Acta 29:335
21. Holland TJB, Redfern SAT (1997) Mineral Mag 61:65
22. Garcia-Muñoz JL, Rodriguez-Carvajal J, Lacorre P, Torrance JB (1992) Phys Rev B 46:4414
23. Pourbaix M (1974) Atlas of electrochemical equilibria in aqueous solutions, 2nd edn. NACE, Houston, pp 330–333
24. Beden B, Bewick A (1998) Electrochim Acta 33:1695
25. Da Silva LM, De Faria LA, Boodts JFC (2001) Electrochim Acta 47:395
26. Levine S, Smith AL (1971) Faraday Discuss Chem Soc 52:290
27. Trasatti S, Petrii O (1991) Pure Appl Chem 63:711
28. Trasatti S (1994) In: Lipkowski J, Ross PN (eds) Electrochemistry of novel materials. VCH, New York, pp 210–211
29. El Baydi M, Tiwari SK, Singh RN (1995) J Solid State Chem 116:157
30. Trasatti S (1991) Electrochim Acta 36:225
31. Jurczalowski R, Hitz C, Lasia A (2004) J Electroanal Chem 572:355